Raman study at high pressure and the thermodynamic properties of corundum: Application of Kieffer's model

Ji-an Xu, Eugene Huang

Institute of Earth Sciences, Academia Sinica, Nankang, Taipei 11529, Taiwan

Jung-fu Lin

Department of Earth Sciences, National Cheng Kung University, Tainan 70101, Taiwan

Lilian Yunyi Xu

Department of Electric Engineering, University of Texas at Austin, Austin, Texas 78712, U.S.A.

Abstract

A Raman spectroscopic study was performed in a diamond-anvil cell to measure the optical vibrational modes of corundum as a function of pressure up to 20 GPa. The integrals concerning the optic continuum in Kieffer's model can be calculated as the weighted sum of each mode in the continuum. Thus, on the basis of Kieffer's model and the experimental results of this study, thermodynamic parameters such as heat capacity, entropy, thermal expansion coefficient, and Gruneisen parameter for corundum at various pressures and temperatures were determined. The contribution to the heat capacity of corundum approaches the classic (Dulong-Petit) limit in the interior of the Earth beneath a depth of 50 km.

Introduction

The theoretical vibrational spectrum of corundum, Al_2O_3, was studied extensively. The space group of corundum is D_{3d}^6 with $Z = 2$ per unit cell. The Al atoms are octahedrally coordinated with two layers of O atoms. Except for three acoustic modes, the irreducible representations for the optical modes in the crystal are $2A_{1g} + 2A_{1u} + 3A_{2g} + 2A_{2u} + 5E_g + 4E_u$.

Among these optical modes, $2A_{1u}$ and $3A_{2g}$ are neither Raman active nor infrared active. On the other hand, the seven Raman-active modes ($2A_{1g} + 5E_g$) and six infrared-active modes ($2A_{2u} + 4E_u$) were detected in previous experiments (Porto and Krishnan, 1967; Gervais and Piriou, 1974).

Raman spectroscopic studies provide information about lattice vibration for an understanding of the thermodynamic properties of solids. Although a detailed lattice dynamics analysis has been conducted (Iishi, 1978), not many Raman measurements of corundum have ever been completed because of the much weaker intensity of corundum (the Raman effect is 10^{-3} times weaker than that of diamond; see Porto and Krishnan, 1967). Such a measurement becomes even more difficult if it is performed at high pressure; hence, only a few experimental measurements with a pressure of up to 1 GPa have been reported (Shin et al., 1976; Watson et al., 1981).

A thermodynamic calculation for corundum at atmospheric pressure was performed by McMillan and Ross (1987) using Kieffer's model, and the results are in good agreement with experimental observation. However, such a study at high pressure has not yet been reported.

The thermal properties in the interior of the Earth are directly related to the heat capacities of its constituent minerals at various high-temperature and high-pressure environments. Although for a long time the classic point of view has been used to deal with the problem, one question has always remained: to what extent does high pressure affect the thermal properties of minerals (Anderson, 1989)? The authors herein attempt to answer the question as it concerns corundum.

Kieffer's Model

Kieffer's model has been used successfully in the calculation of the thermodynamic parameters of various minerals since it was first proposed more than ten years ago (Kieffer, 1979a, 1979b, 1979c, 1980, 1982, 1985). The fundamental basis of this model is the partitioning of the contribution of lattice vibrations by using three frequency distributions for three mode groups: the acoustic, the optic continuum, and the Einstein modes. For the three acoustic modes in a crystal,

$$g(\omega) = (3N_A/Z) \cdot (2/\pi)^3 \{[\sin^{-1}(\omega/\omega_i)]^2/[(\omega_i^2 - \omega^2)^{0.5}]\} \quad (1)$$

where N_A is Avogadro's number, Z is the number of molecules in the Bravais unit cell (two for corundum), and ω_i is the maximum frequency for each mode. For the optic continuum, therefore,

$$g(\omega) = 3N_A n \cdot \{[1 - (1/s) - q]/(\omega_u - \omega_l)\} \quad (2)$$

where ω_l and ω_u are the lower and upper frequency limits in the optic continuum, respectively, n is the number of atoms in the chemical formula (five for corundum), $s =$

$n \cdot Z$ is the total number of atoms in a Bravais unit cell (ten for corundum), and q is the proportion of Einstein vibrational modes (zero for corundum). Similarly for Einstein modes,

$$g(\omega) = 3q N_A n \cdot [\delta(\omega - \omega_{e,i})] \qquad (3)$$

where $\delta(\omega - \omega_{e,i})$ is the δ function for the Einstein frequency $\omega_{e,i}$. However, in Kieffer's model the Einstein modes are defined as those vibrations that can be considered as the internal modes, such as molecule-like vibrations, and their frequencies are much higher than those observed in the Debye frequency range, which is related to the Si-O and O-H stretching vibrations in silicates and hydrous minerals, respectively (Kieffer, 1980, 1982). In the case of corundum, ω_D (around 1295 cm^{-1}, see Kieffer, 1980) is higher than all observed frequencies, hence no contribution from Einstein modes should be considered, and therefore q is zero.

According to Kieffer's model, all the thermodynamic parameters are expressed as the summation of the contributions from these three groups of modes. As an example, the heat capacity at constant volume C_V and entropy S is calculated by

$$C_V = (3 N_A k/s) \Sigma S_1(x_i)$$
$$+ 3 N_A k \cdot [1 - (1/s) - q] \cdot K_1(x_1, x_u)$$
$$+ 3 N_A k q \Sigma E_1(x_{e,i}) \qquad (4)$$
$$S = (3 N_A k/s) \Sigma S_2(x_i)$$
$$+ 3 N_A k \cdot [1 - (1/s) - q] \cdot K_2(x_1, x_u)$$
$$+ 3 N_A k q \Sigma E_2(x_{e,i}) \qquad (5)$$

where the summations in Equations 4 and 5 are taken for three acoustic modes, and S_1, S_2, K_1, K_2, E_1, and E_2 are the contribution functions from the acoustic, the optic continuum, and the Einstein modes, respectively. These functions are defined by

$$S_1(x_i) = (2/\pi)^3 \int_0^{x_i} \{[\sin^{-1}(x/x_i)]^2 \cdot x^2 \cdot e^x$$
$$\div [(x_i^2 - x^2)^{1/2} \cdot (e^x - 1)^2]\} \, dx \qquad (6)$$

$$S_2(x_i) = (2/\pi)^3 \int_0^{x_i} \{[\sin^{-1}(x/x_i)]^2 \cdot x^2 \cdot e^x$$
$$\div [(x_i^2 - x^2)^{1/2} \cdot (e^x - 1)]\} \, dx$$
$$- \int_0^{x_i} \{[\sin^{-1}(x/x_i)]^2 \cdot [\ln(1 - e^{-x})]$$
$$\div [(x_i^2 - x^2)^{1/2} \cdot (e^x - 1)]\} \, dx \qquad (7)$$

$$K_1(x_1, x_u) = \int_{x_1}^{x_u} \{x^2 \cdot e^x / [(x_u - x_1) \cdot (e^x - 1)^2]\} \, dx \qquad (8)$$

$$K_2(x_1, x_u) = \int_{x_1}^{x_u} \{x / [(x_u - x_1) \cdot (e^x - 1)^2]\} \, dx$$

$$- \int_{x_1}^{x_u} \{[\ln(1 - e^x)]/(x_u - x_1)\} \, dx \qquad (9)$$

$$E_1(x_{e,i}) = x_{e,i}^2 \cdot \exp(x_{e,i})^2 [\exp(x_{e,i}) - 1]^2 \qquad (10)$$

$$E_2(x_{e,i}) = \{x_{e,i} / [\exp(x_{e,i}) - 1]^2\}$$
$$- \ln[1 - \exp(-x_{e,i})] \qquad (11)$$

where $x = h\omega/kT$, $x_i = h\omega_i/kT$, $x_1 = h\omega_1/kT$, $x_u = h\omega_u/kT$, $x_{e,i} = h\omega_{e,i}/kT$, h is Planck's constant, k is Boltzmann's constant, and T is temperature. It is noteworthy that (1) the values of $S_1(x_i)$ listed in the reference (Table 1 in Kieffer, 1979c; and Table 5 in Kieffer, 1985) are three times greater than their exact values, and (2) the expression of $K_2(x_1, x_u)$ in the same reference (Eq. 27 in Kieffer, 1979c) was misprinted with the omission of the term $(x_u - x_1)$.

From all the integrals listed above, it is evident that in this model the contributions from the acoustic and Einstein modes are taken into account individually, whereas the contributions from the optic modes are considered as a uniform packet, the optic continuum (Kieffer, 1979c). The thermodynamic properties that can be derived from these vibrational modes depend only on the lower and upper frequencies (x_1 and x_u) and are independent of all other mode frequencies between these two frequency limits. However, there are several thermodynamic parameters, such as the Gruneisen parameter γ, that can be individually related to each mode. It is also important to understand the contribution of each mode in the optic continuum. For such a purpose, we have shown that if the whole frequency range in optic modes is divided into several subintervals, Kieffer's integral, K_j, equals the weighted sum of the same integral over the subintervals (see Appendix), and that

$$K_j = (\Sigma w_i \cdot K_{j,i})/w$$
$$= \left\{ \Sigma w_i \cdot \int_{x_i}^{x_{i+1}} F(x) \, dx \right\} \Big/ w \qquad (12)$$

where the summation is taken over all subintervals ($i = 1$ to k), and $w = x_u - x_1$, $w_i = x_{i+1} - x_i$. Then, the contribution of each mode in the optic continuum is counted individually. In the present study, the numerical calculation also shows the validity of Equation 12.

EXPERIMENTAL RESULTS ON CORUNDUM UP TO 20 GPa

High-pressure Raman spectroscopic experiments were performed in a diamond-anvil cell (DAC). The diamond anvils (type Ia) used were 1/3 carats with a 16-side culet and a 600 μm flat. The gasket with the original thickness of 250 μm was preindented to about 50 μm, and the sample chamber was 150 μm in diameter. The corundum powder used in the present work was the X-ray diffraction reference-standard material and was purchased from the National Bureau of Standards, U.S. Department of
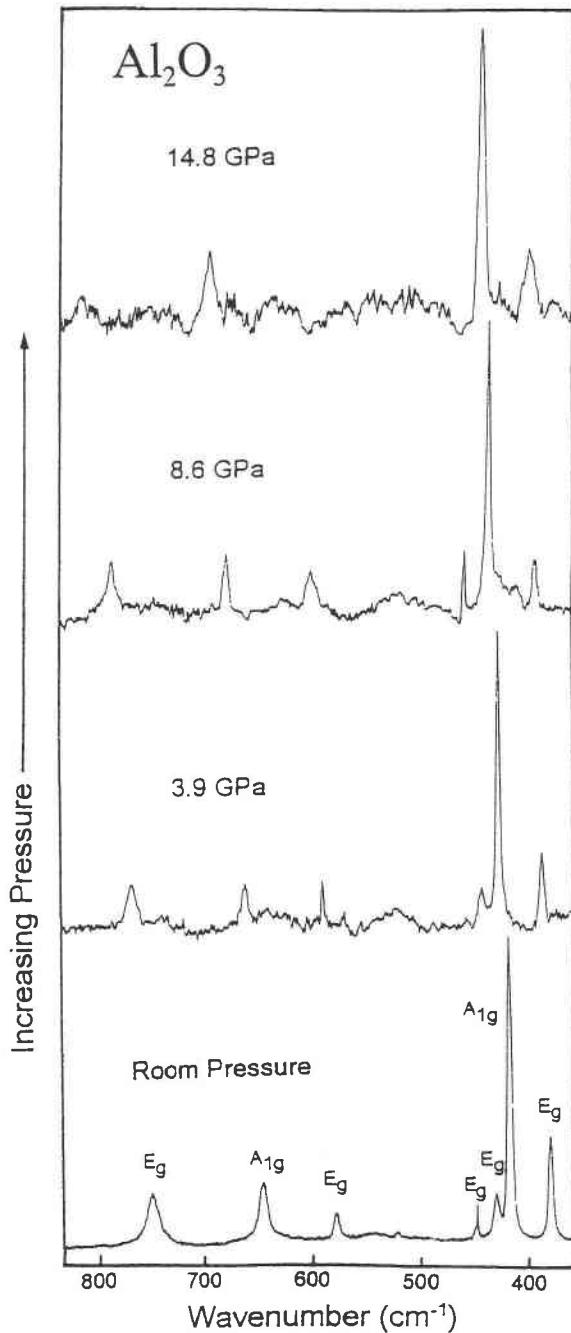
Fig. 1. Experimental records of the Raman spectra of corundum at various pressures.

Fig. 2. Variation of Raman mode frequencies with pressure.

Commerce, Washington, DC. The average grain size of the sample was 0.3 μm. The powder sample was pre-pressed into a disk about 30 μm thick. A piece of a sample cut from the disk was loaded into the sample chamber. A 4:1 methanol-ethanol solution was used as the pressure medium. In this experiment, pressure was measured by averaging at least three pieces of ruby chips in various areas in the sample chamber using the ruby fluorescence method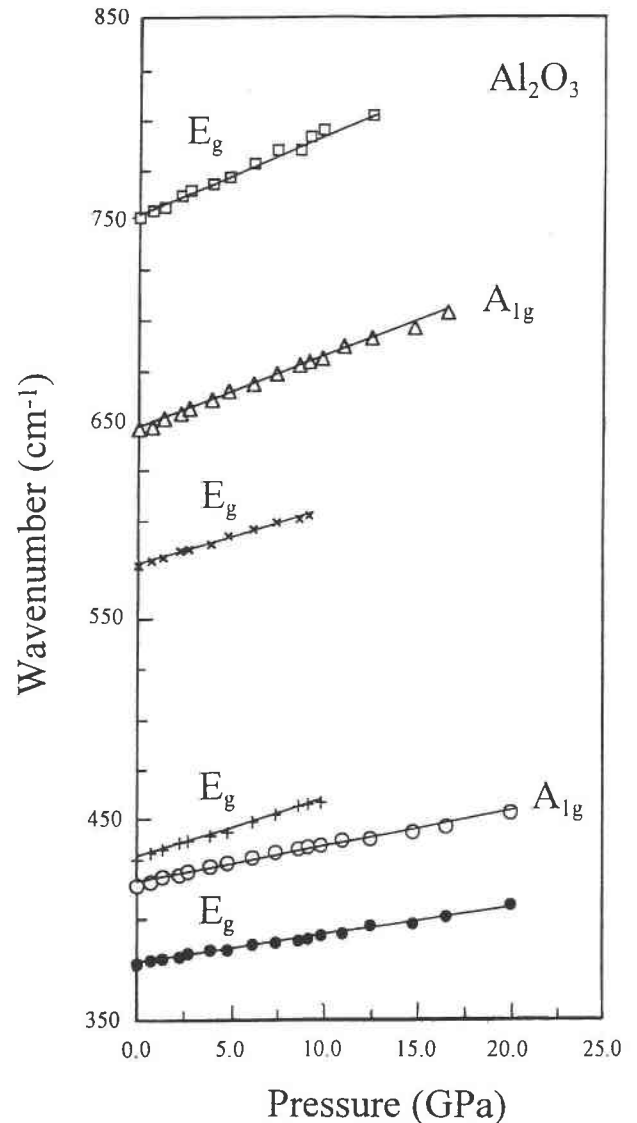 (Mao et al., 1986; Xu et al., 1987). During the experiment, the hydrostatic condition was found to be well maintained when the pressure was under 10 GPa.

Raman measurements were performed in a modular X-Y Dilor system coupled to a CCD detector. A 514.5 nm laser beam, used as an excitation source (Innova 90 Ar$^+$ laser, made by Coherent Company), was focused to about 5 μm on the sample in the DAC. The power of the laser source was 300–500 mW, and the recording time of each Raman spectrum was 20–60 min. The precision in frequency was in the range of 1 cm^{-1}. Details of the experimental procedures can be found in Xu et al. (1990) and Huang et al. (1995).

In the present work, a total of seven Raman-active modes were detected at atmospheric pressure, as shown in Figure 1. However, the weak peak, E_g, at 451.2 cm^{-1} did not appear in high-pressure experiments; thus, only six modes could be measured up to 20 GPa. The results

TABLE 1. The experimental data of mode frequencies at various pressures and comparisons with other reported data on corundum

P (GPa)	Frequency (cm⁻¹)						
	E_g	A_{1g}	E_g	E_g	E_g	A_{1g}	E_g
0.0	377.9	416.6	429.5	451.2	575.9	644.4	749.9
0.7	379.5	416.6	432.5	—	578.3	645.8	753.1
1.4	380.6	418.4	434.5	—	579.5	649.4	754.9
2.2	381.3	420.3	437.8	—	583.3	652.1	760.5
2.7	382.7	421.7	438.8	—	583.9	655.0	763.4
3.9	384.8	423.3	441.3	—	586.3	658.8	766.9
4.8	384.1	427.5	442.8	—	590.9	663.3	770.3
6.0	387.1	429.6	447.4	—	593.7	666.8	776.7
7.3	388.1	432.1	451.1	—	597.7	671.2	783.5
8.6	388.9	433.8	455.4	—	598.9	675.4	783.9
9.1	389.5	434.6	456.0	—	600.9	677.2	790.2
9.8	390.9	436.0	457.2	—	—	679.5	793.4
11.0	392.3	438.8	—	—	—	685.3	—
12.4	396.0	439.6	—	—	—	689.6	801.4
14.8	397.3	443.0	—	—	—	694.1	—
16.6	400.3	445.3	—	—	—	701.5	—
20.0	406.6	451.6	—	—	—	—	—
Parameter							
$(\omega_i)_0$, cm⁻¹	378.4	418.5	430.6	451.2	576.4	645.2	750.6
$d\omega_i/dP$, cm⁻¹/GPa	1.335	1.703	2.794	—	2.760	3.481	4.218
γ_i	0.992	1.148	1.731	—	1.283	1.485	1.517
$(\omega_i)_0$, cm⁻¹*·**	378	418	432	451	578	645	751
$d\omega_i/dP$, cm⁻¹/GPa**	—	2.3	1.7	1.0	1.8	2.7	5.0
$(\omega_i)_0$, cm⁻¹†	378.7	417.4	430.2	448.7	576.7	644.6	750.0
$d\omega_i/dP$, cm⁻¹/GPa†	1.37	2.11	2.95	1.66	2.77	—	4.8

* Porto and Krishnan (1967).
** Shin et al. (1976).
† Watson et al. (1981).

are shown in Figures 1 and 2 and are listed in Table 1. Table 1 also shows that the measured mode frequencies and their pressure dependencies are in good agreement with findings from previous works (Porto and Krishnan, 1967; Shin et al., 1976; Watson et al., 1981).

THERMODYNAMIC PROPERTIES OF CORUNDUM AT HIGH TEMPERATURE UP TO 1800 K

Corundum, in Kieffer's model, is a very interesting material because of the absence of the Einstein mode. In addition, the Debye temperature of corundum (1026 K) is significantly higher than that of most other rock-forming minerals. Hence, the anharmonic effect should not be of importance when the temperature is not too high.

In the present work, the authors attempted to use Kieffer's model to calculate various thermodynamic properties of corundum in high-temperature and high-pressure environments. In these calculations, the data of the acoustic modes were taken from those recommended by Kieffer (1979c). For the optic continuum (x_1, x_u), we used three distribution functions in the calculations: (1) without any subinterval in the range of 300–750.6 cm⁻¹, as recommended by Kieffer (1979c); (2) with six subintervals bounded at 300, 378.4, 418.5, 430.6, 576.4, 645.2, and 750.6 cm⁻¹; and (3) with five subintervals identical to those in (2) except for the low limit (300 cm⁻¹). Those three distributions were denoted as M_1, M_2, and M_3 and are schematically shown in Figure 3. The calculations for M_2 and M_3 were possible because Equation 12 was confirmed mathematically as shown in the Appendix. In the

present study, the shift of optic frequencies with temperatures $\delta\omega/\delta T$, is ignored for following reason: According to findings by Richet et al. (1993), the values of $\delta\omega/\delta T$ of corundum are approximately −0.01 to −0.005 cm⁻¹/K, which are negligible. The initial input parameters for the calculation are listed in Table 2, and the values of $\delta\omega/\delta P$ are listed in Table 1. Therefore, using Kieffer's model, the heat capacity at constant volume, C_V, and entropy, S, at atmospheric pressure up to 1800 K is calculated directly according to Equations 4 and 5.

Gruneisen parameters

As described by Kieffer (1982), the Gruneisen parameter (γ) was taken as the summation of contributions from the three groups

$$\gamma = \gamma_{ac} + \gamma_{op} + \gamma_E \qquad (13)$$

and the γ_{ac}, γ_{op}, and γ_E are defined as the weighted average of each of their respective vibrational modes, $\gamma_{ac} = (\gamma_{ac,1}/C_{V,1}) + (\gamma_{ac,2}/C_{V,2}) + (\gamma_{ac,3}/C_{V,3})$, $\gamma_{op} = (\gamma_{op,1o}/C_{V,1o}) + \ldots + (\gamma_{op,N_o}/C_{V,N_o})$, and $\gamma_E = (\gamma_{e,1e}/C_{V,1e}) + \ldots + (\gamma_{e,N_e}/C_{V,N_e})$, where N_o and N_e are the number of optic and Einstein modes, respectively. N_o varies according to the choice of distribution; it is 2, 7, and 6, respectively, in distributions of M_1, M_2, and M_3. N_e is the total number of Einstein modes; for corundum, N_e is zero.

Part of the numerical results are listed in Table 3 and plotted in Figures 4 and 5. One can see that at ambient conditions, there are no large differences between the calculated Gruneisen parameters using distributions M_2 and
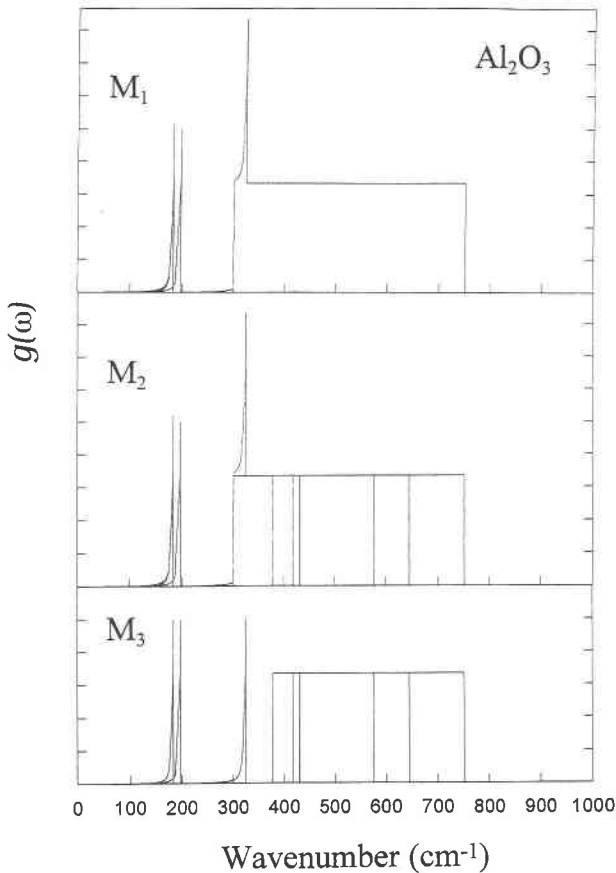
Fig. 3. Three frequency distributions of corundum used in the present study. They are denoted as M_1, M_2, and M_3.

TABLE 3. Parameters of the equation of state of corundum at various pressures

P	$V_0(P)^*$ (cm³/mol)	B (10^{-4}/K)	C (10^{-8}/K²)
0.1 MPa	25.554	0.1827 ± 0.0028	0.1891 ± 0.0133
10.0 GPa	24.641	0.1733 ± 0.0030	0.2026 ± 0.0139
20.0 GPa	23.872	0.1643 ± 0.0031	0.2142 ± 0.0144
30.0 GPa	23.212	0.1554 ± 0.0032	0.2249 ± 0.0150
50.0 GPa	22.123	0.1393 ± 0.0034	0.2427 ± 0.0159
100.0 GPa	20.214	0.1051 ± 0.0036	0.2776 ± 0.0172

* Xu (1987).

Thermal expansion

At ambient conditions, the measured values of the thermal expansion coefficients, α, are between 1.632×10^{-5} (Schreiber and Anderson, 1966) and 2.21×10^{-5} (Touloukian et al., 1977; Zouboulis and Grimditch, 1991). From the calculated Gruneisen parameter γ, the thermal expansion α is calculated directly from

$$\alpha = \gamma \cdot C_V \cdot V/K_T. \qquad (14)$$

The value of the calculated thermal expansion coefficient, 1.403×10^{-5}, is a little smaller than the experimental data listed above. However, it is a stable solution regardless of which of the α values is used as the initial input parameter shown in Table 2. The α, thus determined, is consistent in Kieffer's system.

The calculated value of α is acceptable for two reasons. First, the difference between the calculated value and the experimental data is small, especially taking into account the difficulty of the measurement in high-temperature environments and the error usually introduced during such experiments. Second, the calculated α value in this study is a physically realistic result that approaches zero at a very low temperature, as shown in Figure 5.

Heat capacity at a constant pressure, C_P

The heat capacity at constant pressure, C_P, as a function of temperature up to 1800 K is also determined on the basis of the relationship

$$C_P = C_V(1 + \alpha\gamma T). \qquad (15)$$

The results are listed in Table 3. The experimental data (see McMillan and Ross, 1987) and the calculated values

M_3, with γ close to the experimental value of 1.22–1.33 (Anderson, 1989; Schreiber and Anderson, 1966). On the other hand, the rather small γ value of 0.98 calculated from M_1 was found. Therefore, we believe that the M_2 and M_3 distributions are more acceptable. Consequently, M_2 is used as a working distribution in calculating other thermodynamic properties for corundum in our subsequent study. Similar results obtained in all three distributions showed that it is not necessary to develop a more refined model, as suggested from the work on $MgSiO_3$-ilmenite (Hofmeister and Ito, 1992).

TABLE 2. Initial parameters for calculations on corundum

	Value	d/dT (K^{-1})	d/dP (GPa^{-1})
Molar V (cm³/mol)	25.554*	$2.13 \times 10^{-5**}$	
V of a unit cell (Å³)	84.866*		
Directionally averaged acoustic velocities (km/s): u_1	6.12†	-2.9×10^{-4}†	0.00221†
u_2	6.59	-2.9×10^{-4}	0.00221
u_3	10.85	-3.7×10^{-4}	0.00527
Bulk modulus, K_T (GPa)	255.0*	-0.023‡	4.068*

* Xu (1987).
** Touloukian et al. (1977) and Zouboulis and Grimditch (1991).
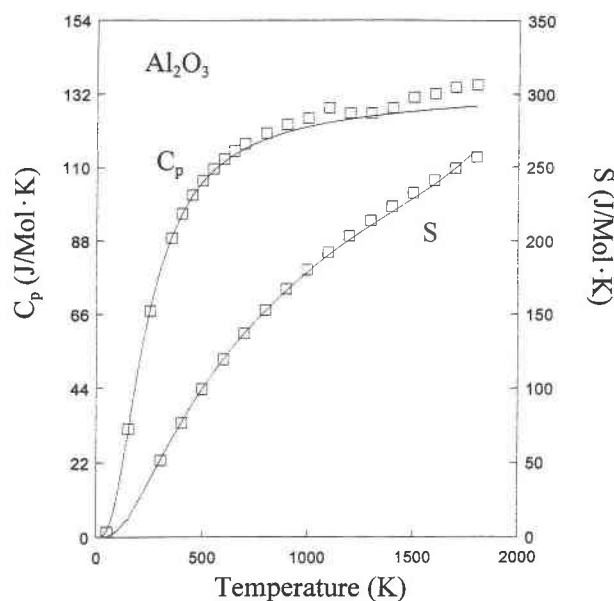† Schreiber and Anderson (1966).
‡ McMillan and Ross (1987).

Fig. 4. Comparison of the calculated (solid lines) and experimental (open squares) heat capacities (C_P) and entropies (S) of corundum at atmospheric pressure and temperatures up to 1800 K.

Fig. 5. Comparison of the calculated (solid lines) and experimental (open squares) coefficient of thermal expansion (α) and Gruneisen parameter (γ) for corundum at atmospheric pressure and temperatures up to 1800 K. Thermal expansion approaches zero when temperature is close to zero.

using various distributions (M_1, M_2, and M_3) on C_P and S are in excellent agreement, as reported previously (Mc-Millan and Ross, 1987). For simplicity, only the results calculated using distribution M_2 are compared with the experimental data (Fig. 4). The minor difference in the high-temperature region between the experimental data and calculation of C_P is due to the departure of the experimental data from the theoretically accepted value (Dulong-Petit value). Such behavior was considered as anharmonicity (Gillet et al., 1991; Fiquet et al., 1992; Reynard and Guyot, 1994), which can be accounted for using anharmonic parameters. However, as described by Richet et al. (1993) for corundum, the anharmonic contributions from various Raman-active modes are, indeed, competing and thus cancel each other. The actual anharmonic behavior should be found from the other (non-Raman-active) modes.

THERMODYNAMIC PROPERTIES OF CORUNDUM AT HIGH PRESSURE UP TO 100 GPa

The contribution of pressure to thermodynamic properties, such as heat capacity from the acoustic mode, has a dual effect. First, the material reduces its molar volume, thereby increasing the V_R and K_{max} under compression (see Kieffer, 1979c); in addition, the experimental results show that the frequencies of various modes, u_i (hence, x_i), normally increase with pressure. Both effects result in a decrease in Kieffer's integral S_1, which in turn results in a decrease in the value of C_V. Similarly, the contributions to C_V resulting from the optic modes are affected less by pressure as their frequencies increase.

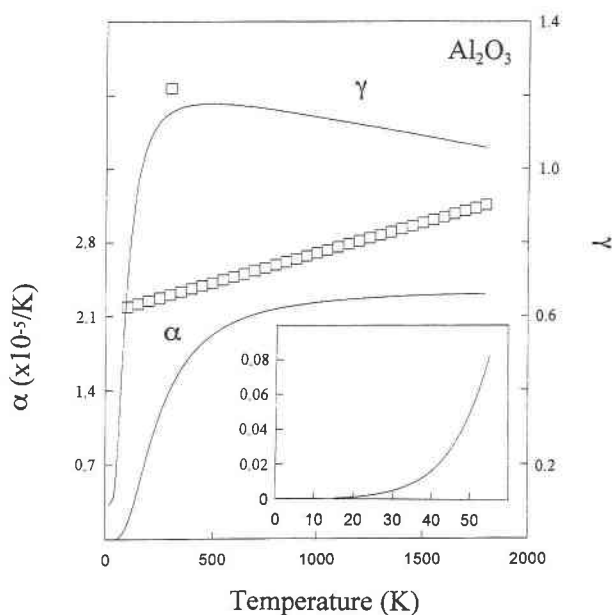On the basis of the justification of Kieffer's model, this calculation can be extended to a much higher pressure region. Although several research groups (Cynn et al., 1990; Marton and Cohen, 1994; Zhang and Bukowinski, 1994) predicted the transformation from corundum phase to Rh_2O_3 (II) phase in the pressure regions of 62, 86–91, and 110–160 GPa, respectively, the experimental data show that corundum is not likely to exhibit a phase transition up to 175 GPa (Xu, 1987; Jephcoat et al., 1988). The heat capacity (C_P), entropy (S), Gruneisen parameter (γ), and thermal expansion coefficient (α) at high pressure up to 100 GPa are calculated accordingly and shown in Figure 6.

The condition that the thermodynamic parameters of C_P, S, and α decrease while γ and $\alpha \cdot K$ increase monotonically with pressure is physically reasonable. In Figure 7, the calculated Gruneisen parameter γ at various pressures and temperatures is plotted against V/V_{298}. A relationship similar to this exists for the change of the Gruneisen parameter with temperature and pressure, except in the case of the change occurring below room temperature. This means that a new mechanism might be needed to account for the discrepancy in the region.

PREDICTION OF EQUATION OF STATE OF CORUNDUM AT HIGH P AND T

From the definition of thermal expansion, $\alpha = (1/V) \cdot (\delta V/\delta T)_P$. Volume, V, at any temperature is determined by

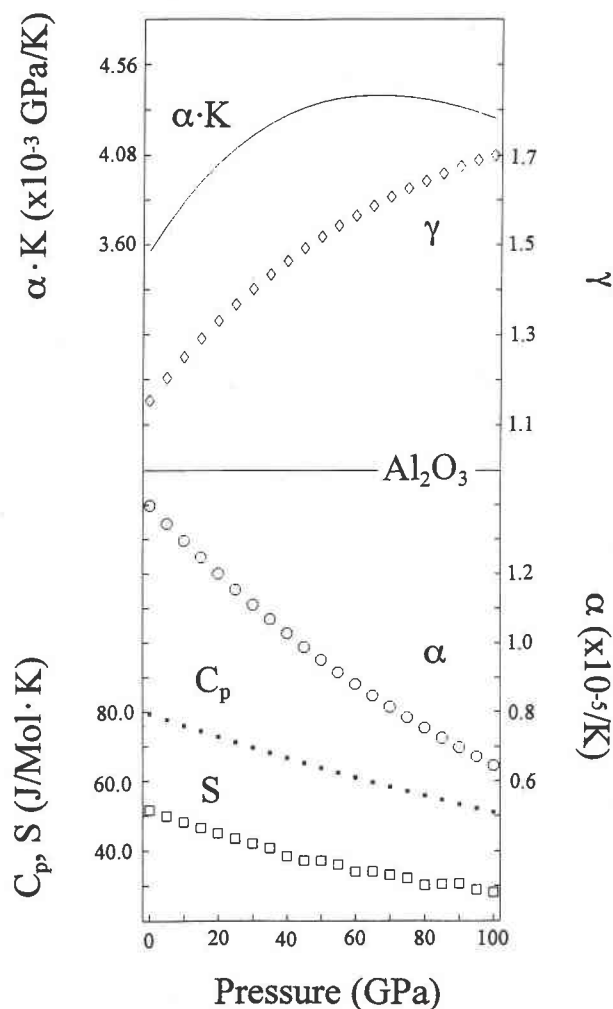$$V = V_{298} + \int_{298}^{T} (V \cdot \alpha)\, dT. \qquad (16)$$

Fig. 6. Thermodynamic parameters of corundum up to 100 GPa at 298 K.

Fig. 7. Gruneisen parameter γ as a function of the volume of corundum by pressure (small squares) and temperature (large squares). It is evident that the hypothesis that the Gruneisen parameter is solely a function of volume (V) is correct except in low-temperature conditions.

Obviously, volume V is determined by iterating Equation 16. More specifically, the volume at 298 K, V_{298}, at various pressures can be used as the initial (first cycle) approximation of the right side of the equation, followed by the first solution V from the left side of Equation 16 as the second approximation. After three to four cycles, a stable solution can thus be determined. Figure 8 shows that a stable solution is obtained at atmospheric pressure after three iterations, although the second iteration is close enough to the final solution. This is, indeed, the equation of state at atmospheric pressure up to 1800 K. Using the same procedure, the equations of state of corundum up to 1800 K can be expressed with good accuracy as

$$V(T,P) = V_0(P) \cdot (1 + BT + CT^2) \qquad (17)$$

where $V_0(P)$ is the volume of corundum at room temperature and various pressures determined experimentally (Xu, 1987). In Table 3, the parameters of the equation of state (B and C in Equation 17) are listed at
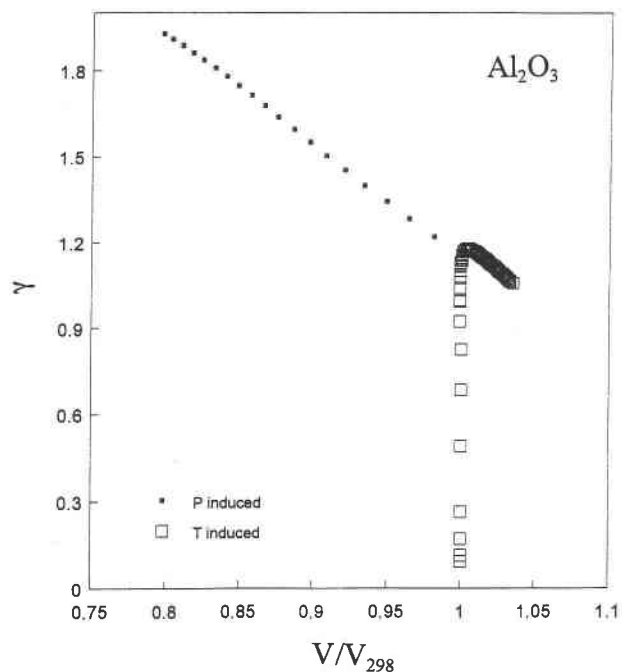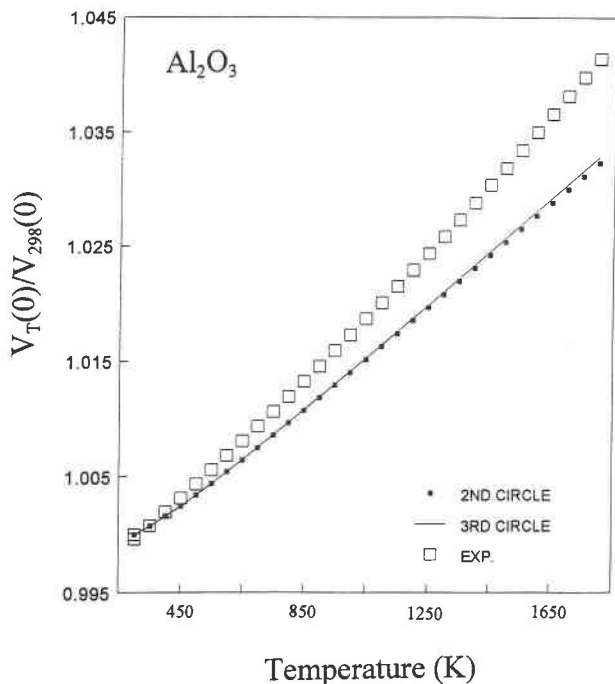

Fig. 8. The calculated equation of state of corundum up to 1800 K at atmospheric pressure. There is a comparison between the experimental data (open squares) and calculated data (solid line). The small squares represent the calculated data in the second cycle of Equation 16. They approximate the final result (solid line).
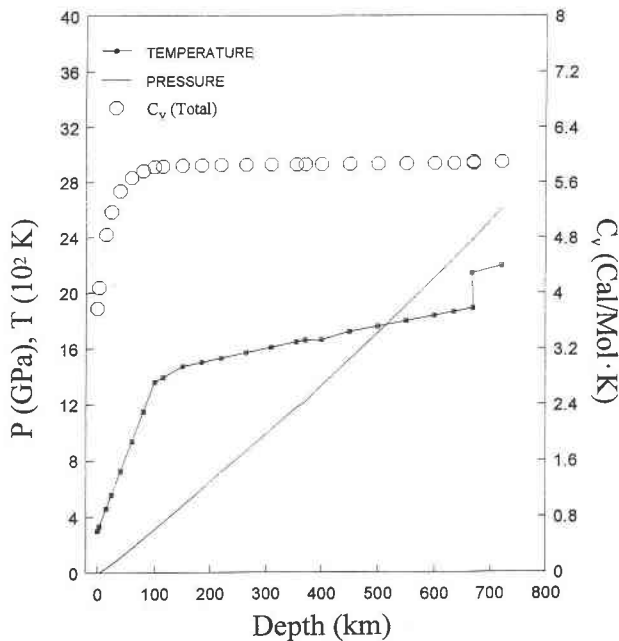
Fig. 9. Heat capacity of corundum approaches its classic (Delong-Petit) value in the interior of the Earth at depths of 50 km or more.

atmospheric pressure, 10, 20, 30, 50, and 100 GPa, respectively.

Although Figure 5 shows a large difference in thermal expansion, α, between the calculated values and the experimental data, the largest discrepancy in V/V_{298} at atmospheric pressure is only about 1% at atmospheric pressure up to 1800 K, as presented in Figure 8.

THE STATUS OF CORUNDUM IN THE EARTH'S INTERIOR

Figure 9 shows the possible temperature and pressure conditions at different depths beneath the Earth's surface (Poirier, 1991), as well as the calculated heat capacity of corundum at various depths up to 800 km. It is interesting to observe that at depths of 50 km or more, the heat capacity of corundum approaches its classic limit (the Dulong-Petit value). Our results show that for a material such as corundum with a relatively high Debye temperature, the temperature at 50 km already makes it behave as a classic material despite pressure. In fact, other materials with a lower Debye temperature would be even more likely to behave as classic materials. Hence, the effect of pressure on heat capacity is much weaker than that of temperature.

We thus conclude that the thermal properties of minerals in the interior of the Earth may be estimated from the classical point of view with sufficient accuracy, provided that the effect of pressure on the constituting minerals is of the same magnitude as that which occurs in corundum.

REFERENCES CITED

Anderson, D.L. (1989) Theory of the Earth, p. 85 and 112. Blackwell Scientific, Boston.

Cynn, H., Isaak, D.G., Cohen, R.E., Nicol, M.F., and Anderson, O.L. (1990) A high-pressure phase transition of corundum predicted by the potential induced breathing model. American Mineralogist, 75, 439–442.

Fiquet, G., Gillet, P., and Richet, P. (1992) Anharmonicity and high-temperature heat capacity of crystals: The example of Ca_2GeO_4, Mg_2GeO_4 and $CaMgGeO_4$ olivines. Physics and Chemistry of Minerals, 18, 469–479.

Gervais, F., and Piriou, B. (1974) Anharmonicity in several-polar-mode crystals: Adjusting phonon self-energy of LO and TO modes in Al_2O_3 and TiO_2 to fit infrared reflectivity. Journal of Physics C: Solid State Physics, 7, 2374–2386.

Gillet, P., Richet, P., Guyot, F., and Fiquet, G. (1991) High temperature thermodynamic properties of forsterite. Journal of Geophysical Research, 96, 11805–11816.

Hofmeister, A.M., and Ito, E. (1992) Thermodynamic properties of $MgSiO_3$ ilmenite from vibrational spectra. Physics and Chemistry of Minerals, 18, 423–432.

Huang, E., Lin, J.F., Xu, J., and Yu, S.C. (1995) Raman spectroscopic studies of diaspore up to 25 GPa. Journal of Geological Society of China, 38, 25–35.

Iishi, K. (1978) Lattice dynamics of corundum. Physics and Chemistry of Minerals, 3, 1–10.

Jephcoat, A.P., Hemley, R.J., and Mao, H.K. (1988) X-ray diffraction of ruby (Al_2O_3:Cr^{3+}) to 175 GPa. Physica, B-150, 115–121.

Kieffer, S.W. (1979a) Thermodynamics and lattice vibrations of minerals: I. Mineral heat capacities and their relationships to simple lattice vibrational modes. Reviews of Geophysics and Space Physics, 17, 1–19.

——— (1979b) Thermodynamics and lattice vibrations of minerals: II. Vibrational characteristics of silicates. Reviews of Geophysics and Space Physics, 17, 20–34.

——— (1979c) Thermodynamics and lattice vibrations of minerals: III. Lattice dynamics and an approximation for minerals with application to simple substances and framework silicates. Reviews of Geophysics and Space Physics, 17, 35–59.

——— (1980) Thermodynamics and lattice vibrations of minerals: IV. Application to chain and sheet silicates and orthosilicates. Reviews of Geophysics and Space Physics, 18, 862–886.

——— (1982) Thermodynamics and lattice vibrations of minerals: V. Applications to phase equilibria, isotopic fractionation, and high pressure thermodynamic properties. Reviews of Geophysics and Space Physics, 17, 827–849.

——— (1985) Heat capacity and entropy: Systematic relations to lattice vibrations. In Mineralogical Society of America Reviews in Mineralogy, 14, 65–127.

Mao, H.K., Xu, J., and Bell, P.M. (1986) Calibration of the ruby pressure to 800 kbar under quasi-hydrostatic conditions. Journal of Geophysical Research, 91, 4673–4676.

Marton, F.C., and Cohen, R.E. (1994) Prediction of a high-pressure phase transition in Al_2O_3. American Mineralogist, 79, 789–792.

McMillan, P., and Ross, N. (1987) Heat capacity calculations for Al_2O_3 corundum and $MgSiO_3$ ilmenite. Physics and Chemistry of Minerals, 14, 225–234.

Poirier, J.-P. (1991) Introduction to the physics of the Earth's interior, p. 211–214 and 236–237. Cambridge University Press, Cambridge.

Porto, S.P.S., and Krishnan, R.S. (1967) Raman effect of corundum. Journal of Chemical Physics, 47, 1009–1012.

Reynard, B., and Guyot, F. (1994) High-temperature properties of gei-kielite (MgTiO$_3$-ilmenite) from high-temperature high-pressure Raman spectroscopy: Some implications for MgSiO$_3$-ilmenite. Physics and Chemistry of Minerals, 21, 441–450.

Richet, P., Gillet, P., Pierre A., Ali Bouhifd, M., Daniel, I., and Fiquet, G. (1993) Raman spectroscopic, X-ray diffraction, and phase relation-ship determinations with a versatile heating cell for measurements up to 3600 K (or 2700 K in air). Journal of Applied Physics, 74, 5451–5456.

Schreiber, E., and Anderson, O.L. (1966) The pressure derivatives of the sound velocities of polycrystalline alumina. Journal of the American Ceramic Society, 49, 184–190.

Shin, S., Pollak, F.H., and Raccah, P.M. (1976) Effects of uniaxial stress on the Raman frequencies of Ti$_2$O$_3$ and Al$_2$O$_3$. In M. Balkanski, R.C.C. Leite, and S.P.S. Porto, Eds., Proceedings of the third international conference on light scattering in solids, p. 401–405. Wiley, New York.

Touloukian, Y.S., Kirby, R.K., Taylor, R.E., and Lee, Y.T.R. (1977) Thermophysical properties of matter, vol. 13: Thermal expansion: Non-metallic solids, p. 176–193. Plenum, New York.

Watson, G.H., Daniels, W.B., and Wang, C.S. (1981) Frequencies in sap-phire. Journal of Applied Physics, 52, 956–958.

Xu, J. (1987) Pressure calibration with argon and the equation of state of ruby up to 600 kbar. High Temperatures—High Pressures, 19, 661–664.

Xu, J., Mao, H.K., and Bell, P.M. (1987) The pressure calibration up to Mbars and the achievement of 5.5 Mbar pressures. Acta Physica Sinica, 36, 500–512.

Xu, J., Wang, S., Manghnani, M.H., Ming, L.C., and Balogh, J. (1990) High pressure Raman study of PbMoO$_4$. In W.B. Holzapfel and P.G. Johannsen, Eds., High pressure science and technology, p. 254–256. Gordon/Breach Science, New York.

Zhang, H., and Bukowinski, M. (1994) Phase transition in Al$_2$O$_3$ revised. Eos, 75(44), 634.

Zouboulis, E.S., and Grimditch, M. (1991) Refractive index and elastic properties of single-crystal corundum (α-Al$_2$O$_3$) up to 2100 K. Journal of Applied Physics, 70, 772–776.

APPENDIX: THE PROPERTY OF KIEFFER'S FUNCTION K_j

Kieffer's function $K_j(x_1, x_u)$ for heat-capacity calculation is defined as the integral for the optic mode in the interval $[x_1, x_u]$, i.e.,

$$K_j(x_1, x_u) = \int_{x_1}^{x_u} \{(x^2 \cdot e^x)/[(x_u - x_1)(\exp(x) - 1)]\}\, dx.$$

Let $F(x) = x^2 e^x/(e^x - 1)$, then

$$K_j(x_1, x_u) = \int_{x_1}^{x_u} [F(x)/(x_u - x_1)]\, dx.$$

If the interval $[x_1, x_u]$ is partitioned into k subintervals as $[x_1, x_1], [x_1, x_2], \ldots, [x_k, x_u]$, it may be confirmed that, for any function $F(x)$, the integral equals the weight summation of every sub-Kieffer integral in its subintervals, namely: $w_i = x_{i+1} - x_i$, $w = x_u - x_1$, and

$$K_{j,i}(x_i, x_{i+1}) = \int_{x_i}^{x_{i+1}} [F(x)/(x_{i+1} - x_i)]\, dx$$

$$= \int_{x_i}^{x_{i+1}} [F(x)\, dx]/w_i$$

$$\Sigma\, w_i \cdot K_{j,i} = \Sigma \int_{x_i}^{x_{i+1}} F(x)\, dx$$

$$= \int_{x_1}^{x_u} F(x)\, dx = K_j \cdot w.$$